

Effects of cooling and heating sources properties and working fluid selection on cryogenic organic Rankine cycle for LNG cold energy utilization

Tianbiao He ^{a,b}, Huigang Ma ^a, Jie Ma ^a, Ning Mao ^{a,b}, Zuming Liu ^{c,*}

^a Department of Gas Engineering, College of Pipeline and Civil Engineering, China University of Petroleum (East China), Qingdao 266580, China

^b Shandong Provincial Key Laboratory of Oil & Gas Storage and Transportation Safety, Qingdao 266580, China

^c Department of Chemical and Biomolecular Engineering, National University of Singapore, Singapore 117585, Singapore



ARTICLE INFO

Keywords:

LNG
Organic Rankine cycle
Cold energy
Mixed working fluid
Optimization

ABSTRACT

Cryogenic organic Rankine cycle (ORC) is considered as one of the most attractive solutions to utilize LNG cold energy for power generation. However, its thermodynamic performance is affected by cooling and heating sources and working fluid selection significantly. Thus, it is crucial to quantify the effects of these factors on cryogenic ORC performance. In this work, we proposed a single-stage cryogenic ORC system to utilize LNG cold energy for sustainable power generation. The effects of LNG vaporization pressure, seawater temperature, minimum temperature approach (MTA), and working fluid selection on cryogenic ORC performance were explored quantitatively. The proposed system adopting different single working fluids and binary working fluids was optimized by particle swarm optimization algorithm to maximize specific net power output (SNPO) with respective to different cooling and heating source properties. The results indicated that the LNG vaporization pressure had the most significant influence on ORC performance. Moreover, R1270 exhibited the highest SNPO (89.34 kJ/kg) and exergy efficiency (18.96%), while C₂H₆ showed the highest thermal efficiency (14.51%). The overall performance was improved significantly by using R1270 and C₂H₆ (30% and 70%) as binary mixture working fluid at 4000 kPa LNG vaporization pressure. However, performance intensification was marginal for a higher LNG vaporization pressure. These results revealed that binary working fluids were not always superior to single working fluids. Hence, this study provided valuable insights on choosing proper working fluids and optimizing design parameters for cryogenic ORC at different operation conditions.

1. Introduction

With the development of economy and deterioration of the environment, the demand of clean and sustainable power generation technologies has increased significantly [1]. Natural gas, as a cleaner fossil fuel, has been widely utilized in natural gas power plants [2]. Liquefied natural gas (LNG) is the preferred method for long distance and cross ocean natural gas transportation [3] owing to its high energy density and ease for transport [4]. Therefore, many countries import LNG as the implement of their energy supply systems [5]. As reported by the International Gas Union, the global LNG trade increased by 13% and reached 354.73 million tonnes in 2019 [6]. LNG, as in liquid form, cannot be used directly and needs to be regasified in LNG terminals before sending to distribution networks [7]. A massive cold energy

(around 830 kJ/kg) will be discharged when LNG is heated from -162 °C to 25 °C at 1 atm by absorbing heat from the seawater in vaporizers [8]. However, most of LNG terminals waste these valuable energy source by releasing them into ocean [9]. How to utilize the wasted LNG cold energy to further enhance the LNG supply chain performance becomes an interesting topic.

Recently, LNG cold energy utilization methods, including cryogenic power generation [10], cryogenic carbon dioxide capture [11,12], desalination [13,14], air liquefaction [15], and energy storage [16,17], have received considerable attentions [18]. Among these technologies, cryogenic power generation is one of the most attractive solutions to generate electricity in a sustainable way. Many researchers have designed and proposed numerous systems to generate power by recovering the LNG cold energy. Angelino and Invernizzi [19] investigated the possibility of real gas Brayton cycles to recover LNG physical exergy.

* Corresponding author.

E-mail address: liuz@u.nus.edu (Z. Liu).

Nomenclature		
Acronym		
E	Expander	<i>h</i> Specific enthalpy, kJ/kg
HEX	Heat exchanger	<i>e</i> Specific exergy, kJ/kg
LNG	Liquefied natural gas	<i>P</i> Pressure, kPa
MTA	Minimum temperature approach	<i>s</i> Specific entropy, kJ/(kg·K)
ORC	Organic Rankine cycle	<i>SNPO</i> Specific net power output, kJ/kg
P	Pump	<i>T</i> Temperature, K
PSO	Particle swarm optimization	<i>VF</i> Vapor fraction
SORC-LNG	Single-stage organic Rankine cycle utilizing LNG cold energy	<i>X</i> A vector containing decision variables
WF	Working fluid	<i>x</i> Molar fraction
<i>Superscripts</i>		<i>Subscripts</i>
<i>ph</i>	physical	<i>s</i> Isentropic
<i>ch</i>	chemical	<i>p</i> Product
<i>Symbols</i>		<i>P</i> Pump
\dot{W}	Power, kW	<i>WF</i> Stream of working fluid
\dot{m}	Mass flowrate, kg/h	<i>L</i> Stream of LNG
\dot{Q}	Heat, kW	<i>SW</i> Stream of seawater
\dot{E}	Exergy, kW	<i>0</i> Dead state
\dot{n}	Molar flowrate, kmole/h	<i>in</i> Inlet
η_{en}	Thermal efficiency	<i>q</i> Heat
η_{ceu}	LNG cold exergy utilization efficiency	<i>out</i> Outlet
η_{ex}	Exergy efficiency	<i>i</i> Index of the stream or component in working fluid
ζ	Isentropic efficiency	<i>j</i> Index of the heat flow
		<i>k</i> Index of power
		<i>d</i> Destruction
		<i>u</i> Utilized
		<i>net</i> Net power output
		<i>f</i> Fuel

Using nitrogen as the working fluid, 0.30 MW/(kg/s) of LNG cold utilization was obtained. However, the heat source temperature was up to 800 °C which made it not accessible near LNG terminals. Gómez [20] designed a closed Brayton cycle combined with a steam Rankine cycle to exploit LNG cold exergy for compressor inlet temperature cooling. Moreover, Ghaebi et al. [21] proposed a Kalina cycle to co-generate cooling and power by utilizing LNG cold exergy. The exergy efficiency was 22.51% with the power to cooling ratio of 0.794. Parikhani et al. [22] optimized a cooling, heating, and power multi-generation system based on Kalina cycle driven by LNG cold energy and geothermal heat. The optimal energy efficiency and exergy efficiency was 62.74% and 33.82%, respectively when the geothermal temperature was 160.5 °C. On the other hand, Lee et al. [23] presented a combined steam Rankine cycle and CO₂ organic Rankine cycle to recover the waste heat from a coal power plant and LNG cryogenic exergy. The gross power was increased by 115% compared with the conventional power plant. Although various systems have been adopted to utilize LNG cold energy, the complex configuration of proposed systems bring about operational issues and high capital investments. Therefore, maneuverable systems with simple configuration like organic Rankine cycles (ORCs) are more desirable for this application.

ORC is regarded as the most auspicious thermodynamic cycle to recover LNG cold energy due to its simple configuration [24], ease of operation [25], and abundant selection of working fluid [26]. The ORC consists of expander, condenser, pump, and evaporator, and employs low boiling point substances as working fluid [27]. This underpins its widespread utilization of ORC for cryogenic power generation using LNG cold energy as its heat sink and various thermal sources as its heat source [28]. In recent years, there has been an increasing interest in investigating the effects of cycle configuration, working fluid selection, LNG cold energy property, and heat source temperatures on ORC overall performance [29].

Several studies have been carried out to improve ORC net power output and exergy efficiency. García et al. [30] proposed a cascaded

Rankine cycles followed by direct expansion process to recover the LNG cold exergy to maximize the specific power. They showed that the specific power reached 235 kW/kg-LNG with a pinch point of 2 °C at 30 bar. Moreover, they found that the pinch point had a significant impact on overall power output, but minor impact on exergy efficiency. Bao et al. [31] proposed a two-stage condensation ORC for LNG cold energy utilization. With two condensers at different condensation temperatures, the exergy losses in the condensers could be reduced remarkably. The results indicated that the net power output of the proposed system was 45.27% higher than the traditional ORC system. Sun et al. [32] compared cascade two-stage ORC, parallel two-stage ORC, and two-stage condensation ORC with ten different potential working fluids. By using ammonia as the working fluid under 200 °C of heat source, the two-stage condensation ORC had the highest exergy efficiency of 30.54%. Tomkow and Cholewiński [33] modeled a multi-stage ORC with ethane-krypton binary mixture as working fluid to recover LNG cold energy. The results showed that 9.3% increase in exergy efficiency and 15.4 kWh/t net power output were achieved at 8.5 MPa natural gas distribution pressure.

Working fluid selection has a significant impact on ORC system performance. Sun et al. [34] studied eight potential working fluids and compared the ORC performances at different low-grade waste heat temperatures (50–200 °C) for LNG cold energy utilization. Bao et al. [35] optimized the mixed working fluid components and compositions for ORC simultaneously. Sung and Kim [36] proposed a novel dual-loop ORC system for LNG cold energy and engine waste heat recovery. They employed six single component fluids for high temperature ORC and seven single component fluids for low temperature ORC. He et al. [37] investigated the performance of ORC adopting single working fluid and binary mixed working fluid in a sustainable energy-water nexus process for LNG cold exergy recovery. The results showed that binary mixed working fluid could match heat transfer curves of cold and hot streams better than single working fluid and generate more power and fresh water. Xue et al. [38] optimized a three-stage ORC system employing

binary and ternary mixed working fluid to utilize LNG cold energy, which enhanced ORC thermal and exergy efficiencies by 3.5% and 7.16%, respectively.

As discussed above, many studies employed waste heat as ORC's heat source for cryogenic power generation, while it is usually not available for most of LNG regasification terminals. Since LNG regasification terminals are normally built near the coastal area at different latitudes, seawater with different temperature is widely used as common heat source for regasification and cryogenic power generation. However, previous studies have not dealt with the effect of seawater temperature on ORC performance and optimal working fluid selection. Moreover, LNG vaporization pressure determines its evaporation curve shape which impacts the available amount of LNG cold energy that could provide to ORC system. Currently, the effect of LNG vaporization pressure on ORC performance is studied by fixing its working fluids. However, there is no guarantee that the selected working fluid is optimal for a wide range of LNG vaporization pressures. Furthermore, the minimum temperature approach (MTA) in the evaporator and condenser significantly impacts ORC net power output and exergy efficiency. Nonetheless, to the best of our knowledge, no studies in the open literature have investigated the effect of MTA on ORC performance for LNG cold energy utilization. Finally, how cooling and heating source properties, and heat exchanger design parameter will influence the working fluid selection in ORC is still unknown. All these research gaps should be addressed to bring a comprehensive understanding on ORC performance associated with working fluid selection under different cooling and heating conditions.

This study aims to: (1) conduct a comprehensive study to showcase the effects of LNG and seawater properties as well as working fluid selection on ORC performance for LNG cold energy utilization; (2) reveal the performance intensification possibility by using mixed working fluid in ORC for cryogenic power generation from LNG cold energy. The main contribution of this study is that it quantifies the effects of LNG cold energy property (LNG pressure), heating stream property (seawater

temperature), and heat exchanger design parameter (MTA) on the overall performance of a single cryogenic ORC system with optimal working fluid selection. This work can provide valuable insights and guidance on ORC design and optimization for different LNG vaporization pressures and seawater temperatures.

The remainder of this work is organized as follows. Section 2 presents a single-stage cryogenic ORC system, while Section 3 introduces performance indexes for system evaluation and process optimization. Thermodynamic and exergy analyses are conducted to examine the influences of system design parameters and optimal working fluids for enhancing system performance are discussed in Section 4. Finally, conclusions of this study are drawn in Section 5.

2. System description and assumption

2.1. Single-stage cryogenic ORC system

Fig. 1 illustrates a single-stage cryogenic ORC system employing LNG cold energy as its heat sink and seawater as its heat source (SORC-LNG system). This system consists of LNG regasification process, cryogenic ORC, and seawater heating process. It converts the wasted LNG cold energy to valuable power in a sustainable way and also reduces the greenhouse gas emission. LNG from the storage tank is pressurized to the vaporization pressure by the LNG pump (P2) and converted into vapor (L-3) by absorbing the heat from the ORC working fluid in the condenser (HEX1). However, the temperature of L-3 stream from the condenser is still low and cannot satisfy the temperature requirement of the natural gas distribution network. Thus, an additional heater (HEX3) is used to increase the natural gas temperature by the seawater.

The working principle of cryogenic ORC is similar to the conventional steam Rankine cycle. The cryogenic ORC adopts organic working fluid with a lower boiling point and utilizes cryogenic heat sink. In the cryogenic ORC, the working fluid is pressurized by the WF pump (P1) to the evaporation pressure. Then, the high-pressure working fluid is

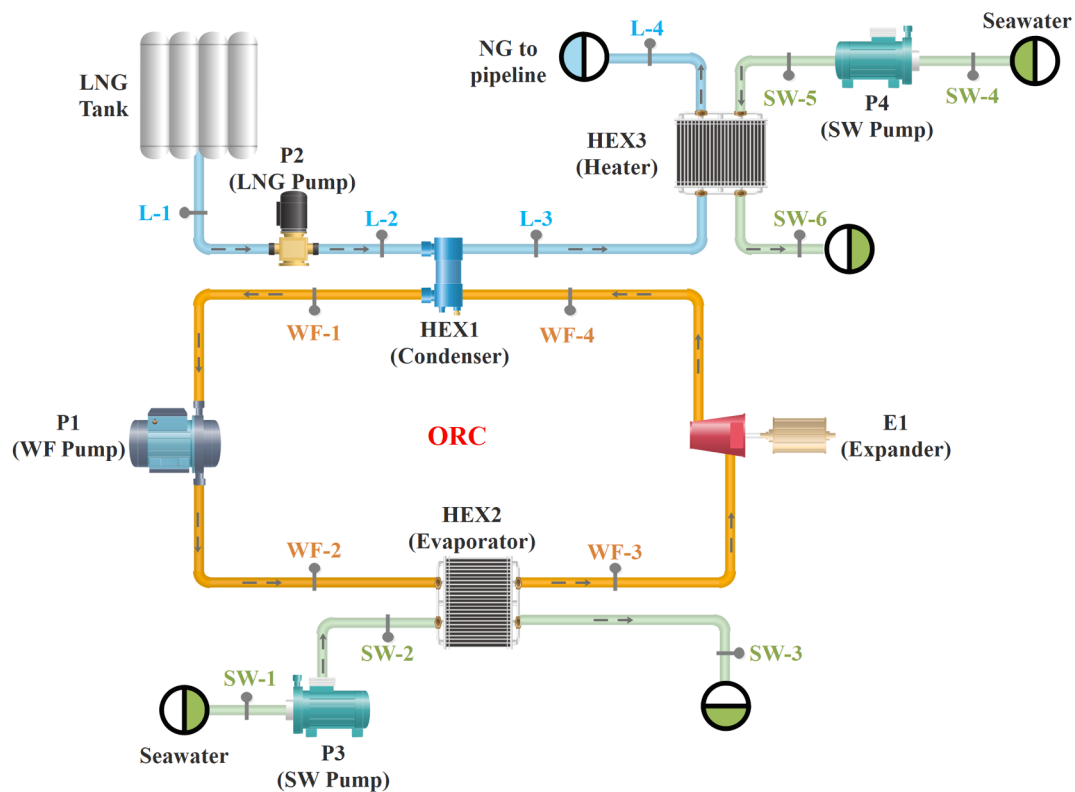


Fig. 1. Schematic representation of the cryogenic ORC system for LNG cold energy utilization.

evaporated in the evaporator by absorbing the heat from the seawater (heat source). The high-pressure and high-temperature working fluid (WF-3) passes through the expander (E1) to reduce its pressure and generate power. Finally, the resulting low-pressure working fluid (WF-4) is condensed by releasing its sensible and latent heat to the LNG (heat sink) and completes the cycle. The seawater is adopted as the heat source of the SORC-LNG system, and is pumped from the ambient pressure to 300 kPa [31] for providing heat to the ORC working fluid in the evaporator (HEX2) and LNG in the heater (HEX3).

2.2. Known parameters and assumptions

The inlet temperature, pressure, and mass flow rate of LNG is -162°C , 101.325 kPa, and 1 kg/s, respectively. The components and compositions of the LNG are shown in Table 1. The investigated LNG vaporization pressures varies from 4000 kPa to 10000 kPa, with a step increase of 1000 kPa. To account for the seasonal variation, the seawater temperatures are assumed to be 15, 20, 25, 30, and 35°C . Moreover, as the MTA of heat exchangers in cryogenic process normally ranging from 2–5 K, they are set to 1, 2, 3, 4, and 5 K in this work, respectively.

Working fluid selection is crucial for the SORC-LNG system because it impacts on the system performance significantly. To explore the effect of working fluid selection on SORC-LNG performance, nine promising single substances and their binary mixtures are considered in this study, as shown in Table 2.

To simplify the simulation and optimization, several assumptions are adopted as follows:

1. The system is at a steady state and thus ignores kinetic and potential energy.
2. The outlet temperature of the natural gas for the distribution network is 10°C [32].
3. The working fluid in the ORC is at subcritical condition.
4. The isentropic efficiency of the pump and expander is 80% and 80%, respectively [31].
5. The discharged temperature of the seawater from HEX2 and HEX3 is assumed to be 5 °C lower than the inlet temperature [38].
6. The pressure drop in the heat changer is 5 kPa [39].
7. The dead states for exergy calculation are 25°C and 101.325 kPa [27].

3. Modeling and optimization

3.1. Process modeling

The SORC-LNG system proposed in this study comprises four pumps, three heat exchangers, and one expander. In this section, energy and exergy analysis are applied to each component in the SORC-LNG system.

3.1.1. Energy analysis

The power consumed by the working fluid pump (P1) is determined by using the following equation:

Table 1
Molar fractions of the LNG [31].

Components	Molar fraction
CH ₄	0.9133
C ₂ H ₆	0.0536
C ₃ H ₈	0.0214
i-C ₄ H ₁₀	0.0047
n-C ₄ H ₁₀	0.0046
i-C ₅ H ₁₂	0.0001
n-C ₅ H ₁₂	0.0001
N ₂	0.0022

Table 2

Potential working fluids for the SORC-LNG system.

Components	Formula	Critical temperature (°C)	Critical pressure (MPa)	Normal boiling temperature (°C)
Ethane	C ₂ H ₆	32.28	4.88	-88.73
Propane	C ₃ H ₈	96.75	4.26	-42.19
Ethylene	C ₂ H ₄	9.21	5.03	-104.09
Carbon dioxide	CO ₂	31.10	7.39	-56.55 *
R1270	C ₃ H ₆	91.06	4.56	-47.62
R134a	C ₂ H ₂ F ₄	101.06	4.06	-26.07
R143a	C ₂ H ₃ F ₃	72.71	3.76	-47.24
R152a	C ₂ H ₄ F ₂	113.26	4.52	-24.02
R23	CHF ₃	26.14	4.83	-82.09

[*] The boiling temperature of CO₂ is at 0.51 MPa.

$$\dot{W}_{P1} = \dot{m}_{WF}(h_{WF-2,s} - h_{WF-1}) = \frac{\dot{m}_{WF}(h_{WF-2} - h_{WF-1})}{\zeta_{p,s}} \quad (1)$$

where \dot{W} , \dot{m} , and h refer to power (kW), mass flowrate (kg/s), and specific enthalpy (kJ/kg), respectively. The subscripts $P1$, WF , $WF-1$, $WF-2$, and s are working fluid pump P1, working fluid, stream WF-1, stream WF-2, and isentropic, respectively. The item $h_{WF-2,s}$ is the specific enthalpy at the pump discharge pressure after an isentropic compression. The Greek symbol $\zeta_{p,s}$ refers to the isentropic efficiency of pumps.

The evaporator (HEX2) is used to transfer the heat from the seawater to the ORC working fluid, turning it into saturate vapor. The heat input to the ORC is given by:

$$\dot{Q}_{HEX2} = \dot{m}_{WF}(h_{WF-3} - h_{WF-2}) = \dot{m}_{SW-2}(h_{SW-3} - h_{SW-2}) \quad (2)$$

where \dot{Q} is the heat flow of the heat exchanger (kW). The subscripts $SW-2$ and $SW-3$ are stream SW-2 and SW-3, respectively.

The expander in the ORC is the key component that determines the power output. The power generated in the expander (E1) is calculated by:

$$\dot{W}_{E1} = \dot{m}_{WF}(h_{WF-4,s} - h_{WF-3}) = \zeta_{e,s}\dot{m}_{WF}(h_{WF-4} - h_{WF-3}) \quad (3)$$

where $\zeta_{e,s}$ refers to the isentropic efficiency of the expander.

The working fluid leaving the expander requires to release its heat to LNG and is condensed into saturate liquid in the condenser. Thus, the heat rejected from the working fluid to the LNG is defined as:

$$\dot{Q}_{HEX1} = \dot{m}_{WF}(h_{WF-1} - h_{WF-4}) = \dot{m}_{LNG}(h_{L-3} - h_{L-2}) \quad (4)$$

The LNG pump is used to increase LNG's pressure to the distribution pressure. The power required by the LNG pump (P2) is given by:

$$\dot{W}_{P2} = \dot{m}_{LNG}(h_{L-2,s} - h_{L-1}) = \frac{\dot{m}_{LNG}(h_{L-2} - h_{L-1})}{\zeta_{p,s}} \quad (5)$$

The power consumed by two seawater pumps (P3 and P4) is defined by Eqs. (6) and (7), respectively.

$$\dot{W}_{P3} = \dot{m}_{SW-2}(h_{SW-3,s} - h_{SW-2}) = \frac{\dot{m}_{SW-2}(h_{SW-3} - h_{SW-2})}{\zeta_{p,s}} \quad (6)$$

$$\dot{W}_{P4} = \dot{m}_{SW-5}(h_{SW-6,s} - h_{SW-5}) = \frac{\dot{m}_{SW-5}(h_{SW-6} - h_{SW-5})}{\zeta_{p,s}} \quad (7)$$

The heater (HEX3) is adopted to rise the natural gas temperature when the temperature of stream L-3 is lower than the specified value for downstream distribution. The heat obtained by LNG is calculated by:

$$\dot{Q}_{HEX3} = \dot{m}_{LNG}(h_{L-4} - h_{L-3}) = \dot{m}_{SW-5}(h_{SW-6} - h_{SW-5}) \quad (8)$$

3.1.2. Exergy analysis

Exergy analysis of a power generation system can quantify the quality of the heat transfer process from the heat source to the heat sink. Neglecting the potential and kinetic exergies, the exergy of each stream is defined by [40]:

$$\dot{E} = \dot{m}e = \dot{m}(e^{ph} + e^{ch}) \quad (9)$$

where \dot{E} and e refer to exergy (kW) and specific exergy (kJ/kg), respectively. The superscripts ph and ch represent physical exergy and chemical exergy, respectively.

Since there is no chemical reaction occurs and no component changes in the proposed system, the chemical exergy does not vary in any process and thus can be ignored. The physical exergy can be given by:

$$e^{ph} = (h - h_0) - T_0(s - s_0) \quad (10)$$

where T and s refer to temperature (K) and specific entropy (kJ/(kg·K)), respectively. The subscript 0 refers to the dead state or the ambient environment.

Exergy destructions are induced by thermodynamic irreversibilities associated with compression, expansion, and heat transfer in the SORC-LNG system. The exergy destruction for each equipment is determined by exergy balance as follows:

$$\sum_{i=1}^I \dot{E}_{in,i} + \sum_{j=1}^J \dot{E}_{q,j} = \sum_{i=1}^I \dot{E}_{out,i} + \sum_{k=1}^K \dot{W}_k + \Delta\dot{E}_d \quad (11)$$

where the subscripts in , out , q , and d denote inlet, outlet, heat, and destruction, respectively. The symbols i, j , and k denote the i th exergy stream, j th exergy associated with heat transfer, and k th power, respectively.

For pumps, exergy destructions are given by:

$$\Delta\dot{E}_d^P = \dot{E}_{in} - \dot{E}_{out} - \dot{W}_P \quad (12)$$

For expander, the exergy destruction is defined as:

$$\Delta\dot{E}_d^E = \dot{E}_{in} - \dot{E}_{out} + \dot{W}_E \quad (13)$$

For heat exchangers, exergy destructions are described by:

$$\Delta\dot{E}_d^{HEX} = \sum_{i=1}^I (\dot{E}_{in,i} - \dot{E}_{out,i}) \quad (14)$$

The exergy destructions of each equipment of the SORC-LNG system are listed in Table 3. By summation the exergy destruction of each equipment, the total exergy destruction of the SORC-LNG system is obtained:

Table 3
Exergy destructions of each equipment of the SORC-LNG system.

Equipment	Exergy destruction equation
Working fluid pump (P1)	$\Delta\dot{E}_d^{P1} = \dot{E}_{WF-2} - \dot{E}_{WF-1} - \dot{W}_P$
LNG pump (P2)	$\Delta\dot{E}_d^{P2} = \dot{E}_{L-2} - \dot{E}_{L-1} - \dot{W}_P$
Seawater pump (P3)	$\Delta\dot{E}_d^{P3} = \dot{E}_{SW-2} - \dot{E}_{SW-1} - \dot{W}_P$
Seawater pump (P4)	$\Delta\dot{E}_d^{P4} = \dot{E}_{SW-5} - \dot{E}_{SW-4} - \dot{W}_P$
Working fluid expander (E1)	$\Delta\dot{E}_d^{E1} = \dot{E}_{WF-4} - \dot{E}_{WF-3} + \dot{W}_E$
Condenser (HEX1)	$\Delta\dot{E}_d^{HEX1} = \dot{E}_{WF-4} - \dot{E}_{WF-3} + \dot{E}_{L-2} - \dot{E}_{L-3}$
Evaporator (HEX2)	$\Delta\dot{E}_d^{HEX2} = \dot{E}_{WF-2} - \dot{E}_{WF-3} + \dot{E}_{SW-2} - \dot{E}_{SW-3}$
Heater (HEX3)	$\Delta\dot{E}_d^{HEX3} = \dot{E}_{L-3} - \dot{E}_{L-4} + \dot{E}_{SW-5} - \dot{E}_{SW-6}$

$$\Delta\dot{E}_d = \Delta\dot{E}_d^{P1} + \Delta\dot{E}_d^{P2} + \Delta\dot{E}_d^{P3} + \Delta\dot{E}_d^{P4} + \Delta\dot{E}_d^{E1} + \Delta\dot{E}_d^{HEX1} + \Delta\dot{E}_d^{HEX2} + \Delta\dot{E}_d^{HEX3} \quad (15)$$

3.2. Performance indicator

In this section, several key process performance indicators are used to evaluate the performance of the SORC-LNG system.

Conventionally, the net power output is adopted to estimate the performance of the cryogenic power generation system for LNG cold energy utilization. However, the value of the net power output varies with the flowrate of LNG, making it difficult to compare the performance of different systems. Thus, the specific net power output (SNPO) is introduced as the first indicator in this study. The definition of the SNPO is the ratio of the net power output to the mass flowrate of LNG, as described in Eq. (16).

$$SNPO = \frac{\dot{W}_{net}}{\dot{m}_{LNG}} \quad (16)$$

where \dot{W}_{net} refers to the net power output of the SORC-LNG system, which is given by:

$$\dot{W}_{net} = \dot{W}_{E1} - \dot{W}_{P1} - \dot{W}_{P2} - \dot{W}_{P3} - \dot{W}_{P4} \quad (17)$$

The second indicator is the thermal efficiency, which reflects the capability of the heat engine converting heat to power, as described in Eq. (18).

$$\eta_{en} = \frac{\dot{W}_{net}}{\dot{Q}_{in}} = \frac{\dot{W}_{net}}{\dot{Q}_{HEX2}} \quad (18)$$

LNG cold exergy utilization efficiency, as the third indicator, can be used to evaluate the heat transfer efficiency of the condenser. If the LNG cold exergy is totally utilized by the SORC-LNG system, the LNG cold exergy utilization efficiency equals to 1. Otherwise, a fraction of the LNG cold exergy is wasted. It is defined as the ratio of the utilized cold exergy in the condenser to the total provided cold exergy to the system, which is given by Eq. (19):

$$\eta_{ceu} = \frac{\dot{E}_u}{\dot{E}_{LNG,in} - \dot{E}_{LNG,out}} = \frac{\dot{E}_{WF-1} - \dot{E}_{WF-4}}{\dot{E}_{L-2} - \dot{E}_{L-4}} \quad (19)$$

Exergy efficiency is the ratio of the product exergy to the fuel exergy. For the SORC-LNG system, the most important fuel exergy is the LNG cold exergy and the product exergy is the net power output. Thus, by ignoring the fuel exergy of the seawater, the exergy efficiency is given by:

$$\eta_{ex} = \frac{\dot{E}_p}{\dot{E}_f} = \frac{\dot{W}_{net}}{\Delta\dot{E}_{LNG}} \quad (20)$$

3.3. Process optimization

The SORC-LNG system is modeled in a process simulator Aspen HYSYS V10 [41]. The thermodynamic properties of the LNG and working fluid are calculated by the Peng-Robinson equation of state [42], while those of the seawater are calculated by the Electrolyte NRTL equation of state [43].

The optimization is implemented in Matlab [44] by using Particle Swarm Optimization algorithm (PSO). Matlab can interactively with Aspen HYSYS via ActiveX to exchange data [17]. The flow chart of the optimization process is shown in Fig. 2.

In this study, the objective is to maximize the SNPO, which can be described as:

$$\max[f(X)] = SNPO \quad (21)$$

The symbol X is a vector consisting of decision variables, namely the

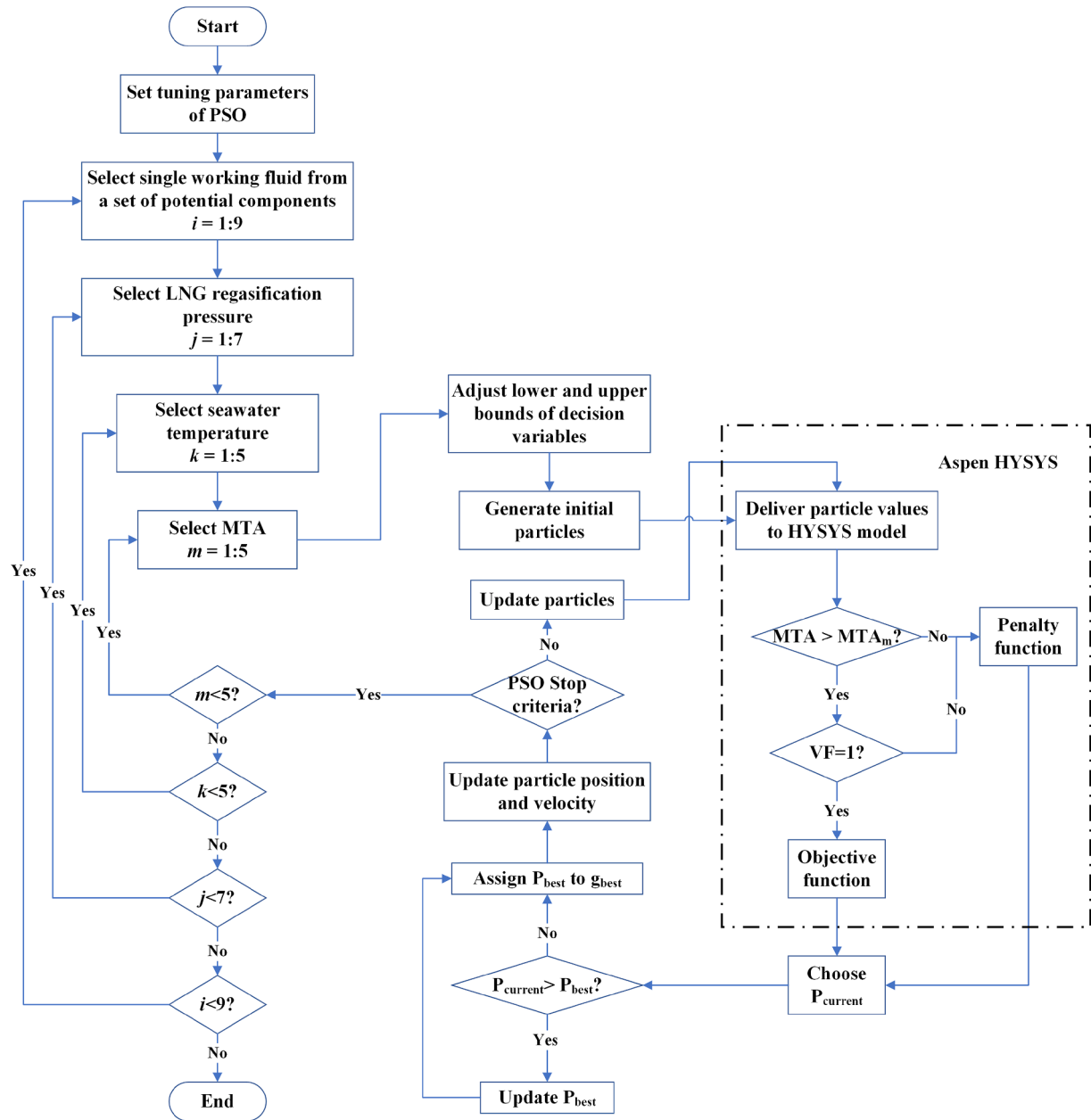


Fig. 2. Flow chart of the particle swarm optimization process.

composition, evaporation pressure, condensation pressure, and molar flow rate of the working fluid, which is given by:

$$X = [x_i, P_{WF-2}, P_{WF-4}, \dot{n}_{WF-1}] \quad (22)$$

where x_i refers to the composition of i th component in the working fluid. If single component is used as the working fluid, $x_i = 1$.

The lower and upper bounds of decision variables are listed in Table 4. Since nine potential working fluids are optimized at different

Table 4
The lower and upper bounds of the decision variables.

Decision variable	Lower bound	Upper bound
x_i	0	1
P_{WF-2} (kPa)	$P_b(T_{SW-3} - MTA)$	P_{cri}
P_{WF-4} (kPa)	110	$P_b(T_{SW-3} - MTA)$
\dot{n}_{WF-1} (kmole/h)	0.01	200

conditions, the search spaces of the decision variables are not specified. For the evaporation pressure, the lower bound is the saturate pressure when the working fluid temperature is ($T_{SW-3} - MTA$) and vapor fraction is 1, while the upper bound is the critical pressure of the working fluid. For the condensation pressure, the lower bound is 110 kPa to avoid the vaccum condition for the system.

Constraints are introduced to avoid the algorithm searching infeasible area and eliminating the undesirable particles. The first constraint is that the MTA of three heat exchangers should be larger or equal to the specified value, which can be described as Eq. (23).

$$MTA_i \geq MTA_s \quad \forall i = (\text{HEX1, HEX2, HEX3}) \quad (23)$$

$$MTA_s \in [1, 2, 3, 4, 5]$$

where MTA_s refers to the specified MTA value, which equals to [1, 2, 3, 4, 5].

The second constraint is that the working fluid entering the expander (stream WF-3) should be saturate vapor without any liquid, as given by

Eq. (24).

$$VF_{WF-3} = 1 \quad (24)$$

where VF refers to the vapor fraction of the stream.

When constraints are violated, the algorithm will use the penalty function to replace the objective function. The penalty function is defined by Eq. (25):

$$p(X) = -SNPO \times e^{100 \times \max(|MTA_s - MTA_f|, |1 - VF_{WF-3}|)} \quad (25)$$

4. Results and discussion

In this section, results are presented concerning the following indicators of comparison: SNPO, thermal efficiency, LNG cold exergy utilization efficiency, and exergy efficiency. The effects of LNG vaporization pressure, seawater temperature, and MTA on the SORC-LNG performance are presented in Section 4.1, 4.2, and 4.3, respectively. In Section 4.4, we investigate the performance of the best single working fluid selected from nine potential substances. The performance enhancements by adopting binary mixed working fluid are discussed in Section 4.5.

4.1. Effect of LNG vaporization pressure on SORC-LNG performance

The LNG vaporization pressure not only determines the maximum available cold exergy that could be provided to the ORC system, but also affects the shape of the evaporation curve, as shown in Fig. 3.

In this section, the seawater temperature and MTA are 25 °C and 3 K, respectively. In Fig. 4, the SNPO, thermal efficiency, LNG cold exergy utilization efficiency, and exergy efficiency are presented, which is varied from 4000 kPa to 10000 kPa. For the nine single working fluids considered here, the SNPO generally decreases with the increase of the LNG vaporization pressure, as illustrated in Fig. 4(a). This is because the available cold exergy for the SORC system decreases with the LNG vaporization pressure, thereby reducing the net power output from the expander. For working fluids such as C₂H₆, C₂H₄, and R23, the SNPO decreases rapidly when the LNG vaporization pressure increases and then the decrements are more flat. Among the nine single working fluids, R1270 shows the highest SNPO (89.34 kJ/kg at 4000 kPa and 38.86 kJ/kg at 10000 kPa).

In the term of the thermal efficiency, the SORC-LNG system is less efficient as the increase of the LNG vaporization pressure. Although the required heat input also decreases with the LNG vaporization pressure, the decrease of the net power output is more rapidly than the required

heat input, leading to the decrease of the thermal efficiency. Obviously, C₂H₆ produces the highest thermal efficiency at 4000 kPa. Although the SNPO of C₂H₆ is significantly lower than R1270 when LNG vaporization pressure is larger than 5000 kPa, the thermal efficiency of C₂H₆ is the highest at different pressures. It is because the evaporation pressure of C₂H₆ is around 3788 kPa and is much higher than that of R1270 (981 kPa), which results in smaller heat input in the evaporator and thus achieves higher thermal efficiency. Moreover, it should be noted that the thermal efficiency difference between C₂H₆ and R1270 reduces with the increase of the LNG vaporization pressure. The thermal efficiency of C₂H₆ and R1270 is 8.29% and 7.88% at 10000 kPa, respectively. For working fluids such as R134a and R152a, their thermal efficiencies are significantly lower than other working fluids. It indicates that these two working fluids are not suitable for the SORC-LNG system from the perspective of thermal efficiency.

LNG cold exergy utilization efficiency reflects the heat transfer efficiency in the condenser. If the working fluid condensation curve matches the LNG evaporation curve properly, the LNG cold exergy utilization efficiency is high, and vice versa. For working fluid such as R143a, R1270 and C₃H₈, the LNG cold exergy utilization efficiency decreases with the LNG vaporization pressure. However, the LNG cold exergy utilization efficiency of C₂H₆, C₂H₄ and R23 first decrease and then increase slightly when the pressure increases from 4000 kPa to 6000 kPa. Moreover, the LNG cold exergy utilization efficiency of R134a and R152a increase firstly and then decrease with the LNG vaporization pressure. The working fluids considered here can be classified into high boiling point (R134a and R152a), medium boiling point (R143a, R1270 and C₃H₈), and low boiling point (C₂H₆, C₂H₄, CO₂ and R23). For high boiling point working fluids, the condensation pressure is limited to 110 kPa which leads to the condensation temperature is around -20 °C and thereby a large gap between the condensation curve and LNG evaporation curve. It can be seen from Fig. 3(b) that the gap between the working fluid condensation curve and LNG evaporation curve reduces firstly and then increases with the increase of LNG vaporization pressure. For low boiling point working fluids, the condensation temperature is close to the turning point on LNG evaporation curve at lower pressure, which results in a small gap between them and a high LNG cold exergy utilization efficiency. The condensation temperature increases significantly with the increase of LNG vaporization pressure (4000 kPa to 6000 kPa), leading to the decrease of LNG cold exergy utilization efficiency. However, at pressure higher than 7000 kPa, the LNG evaporation curve becomes smooth, and thus a smaller gap between the working fluid and LNG and increasing the LNG cold exergy utilization efficiency are observed.

Fig. 4(d) illustrates the variation of exergy efficiency with LNG vaporization pressure. It can be seen that the exergy efficiency decreases with higher LNG vaporization pressure. The exergy efficiency exhibits the similar trends as the SNPO, as shown in Fig. 4(a) and (d). Since the net power output and available LNG cold exergy decrease with the LNG vaporization pressure, their synergistic effects result in the similar trends of the exergy efficiency and SNPO. Moreover, the exergy efficiency of R1270 is the highest among the nine single working fluids.

4.2. Effect of seawater temperature on SORC-LNG performance

Fig. 5 illustrates the effect of seawater temperature on SNPO, thermal efficiency, LNG cold exergy utilization efficiency, and exergy efficiency at 7000 kPa LNG vaporization pressure and 3 K MTA.

The SNPO increases with the increase of the seawater temperature, as shown in Fig. 5(a). This is because the higher seawater temperature leads to higher expander inlet temperature and thereby results in more power generated in the expander. However, the effect of seawater temperature on different working fluids is distinctive. For low boiling point working fluids such as CO₂, C₂H₄, C₂H₆, and R23, the increment of the SNPO is very small. For instance, the SNPO of C₂H₆ increases by 15.45% from 40.27 kW at 15 °C to 46.49 kW at 35 °C. For medium and

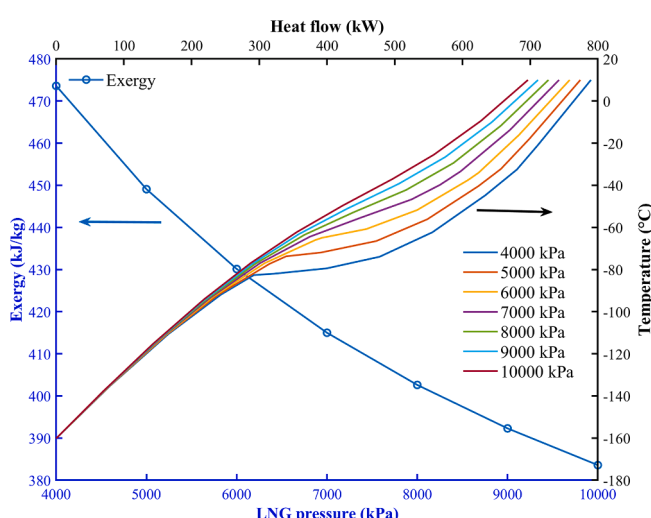


Fig. 3. Maximum available cold exergy and LNG evaporation curve.

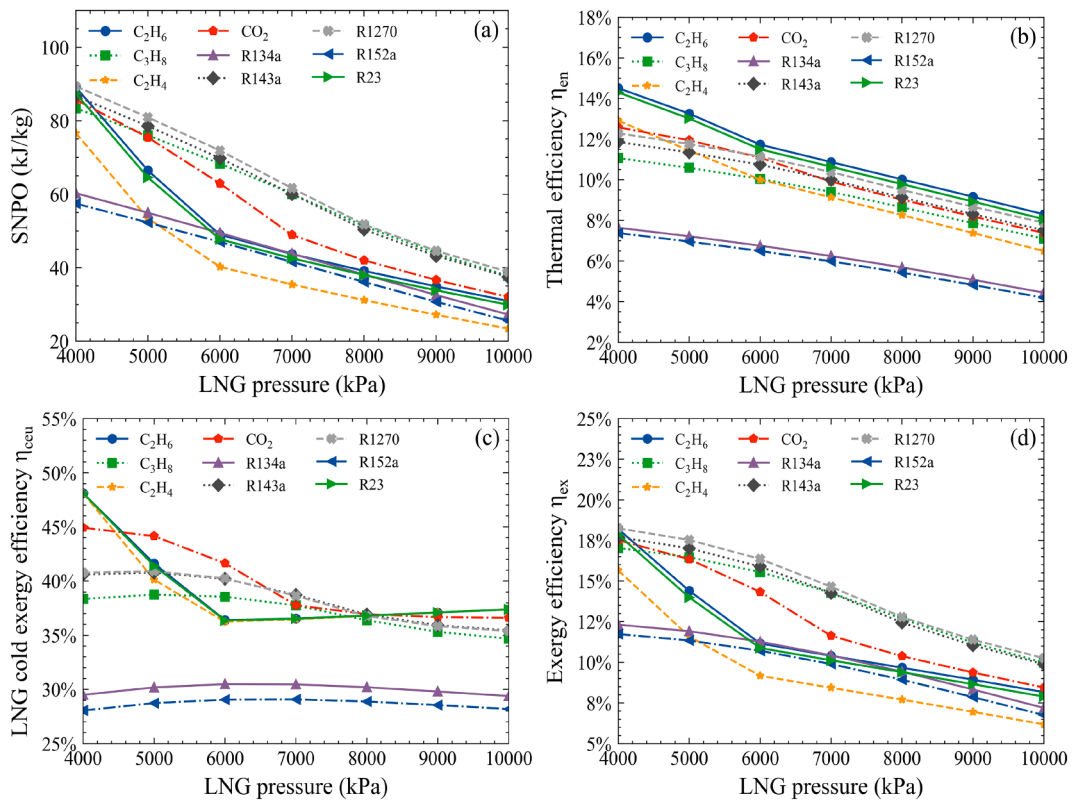


Fig. 4. SNPO (a), thermal efficiency (b), LNG cold exergy utilization efficiency (c) and exergy efficiency (d) as a function of the LNG vaporization pressure for nine potential single-component working fluids and MTA = 3 K and SW T = 25 °C.

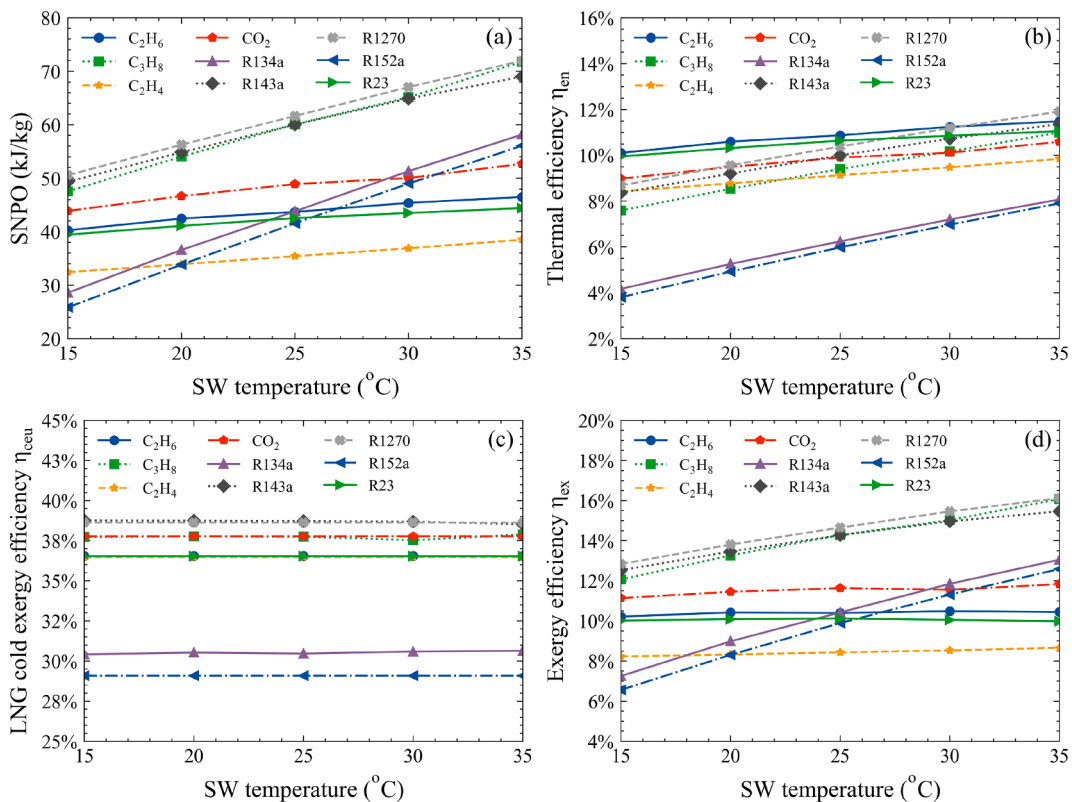


Fig. 5. SNPO (a), thermal efficiency (b), LNG cold exergy utilization efficiency (c) and exergy efficiency (d) for nine potential single-component working fluids and MTA = 3 K and LNG pressure = 7000 kPa.

high boiling point working fluids, the increase of the seawater temperature has significant influences on their SNPOs. The largest SNPO (71.97 kW) is achieved by R1270 at 35 °C seawater temperature.

In terms of the thermal efficiency, the SORC-LNG system is generally more efficient with higher seawater temperature, despite the seawater pumps consume much power to deliver the heat source. When the seawater temperature is lower than 30 °C, C₂H₆ shows the highest thermal efficiency among nine working fluids. However, R1270 surpasses C₂H₆ and holds superior thermal efficiency when the seawater temperature is higher than 30 °C.

In Fig. 5(c), it is clear that the seawater temperature does not impact the LNG cold exergy utilization efficiency significantly. The LNG cold exergy utilization efficiency remains constant irrespective of the seawater temperature. The reason is that the seawater temperature only increases the expander inlet pressure, but the condensation pressure does not affect by the seawater temperature. Thus, the LNG cold exergy utilized by the working fluid in the condenser remains unchanged and this directly results in a constant LNG cold exergy utilization efficiency.

For the exergy efficiency of the SORC-LNG system, it increases with the seawater temperature and has the same trend as the SNPO, as shown in Fig. 5(d). This is because the LNG cold exergy provided to the system keeps constant and the net power output increases with the increase of the seawater temperature. Thus, the exergy efficiency variation curve has the same slope as the SNPO.

4.3. Effect of MTA on SORC-LNG performance

The MTA in the evaporator and condenser of the SORC-LNG system influences the flowrate, evaporation temperature, and condensation temperature of the working fluid. Fig. 6 shows the SNPO, thermal efficiency, LNG cold exergy utilization efficiency and exergy efficiency at 7000 kPa LNG vaporization pressure and 25 °C seawater temperature.

It can be seen that the SNPO decreases with the increase of the MTA

in heat exchangers. The reason is that the flowrate of the working fluid reduces with the increase of the MTA and thus the SNPO decreases. R1270 provides the largest SNPO across all the MTA among nine single working fluids. Its SNPO is 56.80 kW at MTA = 5 K, but is 14.68% lower than that at MTA = 1 K. In addition, C₃H₈ and R143a exhibit the second and third highest SNPO, while C₂H₆ possesses the lowest SNPO (32.65 kW) at MTA = 5 K.

Fig. 6(b) illustrates the variation of the thermal efficiency with the MTA. It is clear that the SORC-LNG system is generally less efficient with a larger MTA. This can be explained from two aspects. One aspect is that the increase of the MTA reduces the evaporation pressure in HEX2 and thereby increases the heat input. However, the working fluid flowrate decreases with the increase of the MTA which tends to decrease the heat input. Due to the larger impact on working fluid flowrate, the required heat input declines slightly with the increase of the MTA. The other aspect is that the net power output decreases with the MTA. These two factors synergistically result in a much flat drop of the thermal efficiency. The system thermal efficiency with C₂H₆ as working fluid is reduced by 6.97% from 11.34% at 1 K MTA to 10.55% at 5 K MTA.

The LNG cold exergy utilization efficiency decreases with the increase of the MTA, as shown in Fig. 6(c). The LNG cold exergy utilization efficiency represents the exergy destruction in HEX1. The larger the MTA, the larger the exergy destruction in HEX1 and thereby a lower utilization efficiency. The LNG cold exergy utilization efficiency of R1270 is the highest across all MTAs which indicates the most efficient heat transfer between R1270 and LNG.

In terms of the exergy efficiency, it has the same trend as the SNPO since the LNG cold exergy provided to the SORC-LNG system does not change with the MTA. The SORC-LNG system adopting R1270 provides the highest exergy efficiency among nine working fluids. The exergy efficiency of R1270 decreases by 14.67% from 16.49% to 14.07% when the MTA raises from 1 K to 5 K.

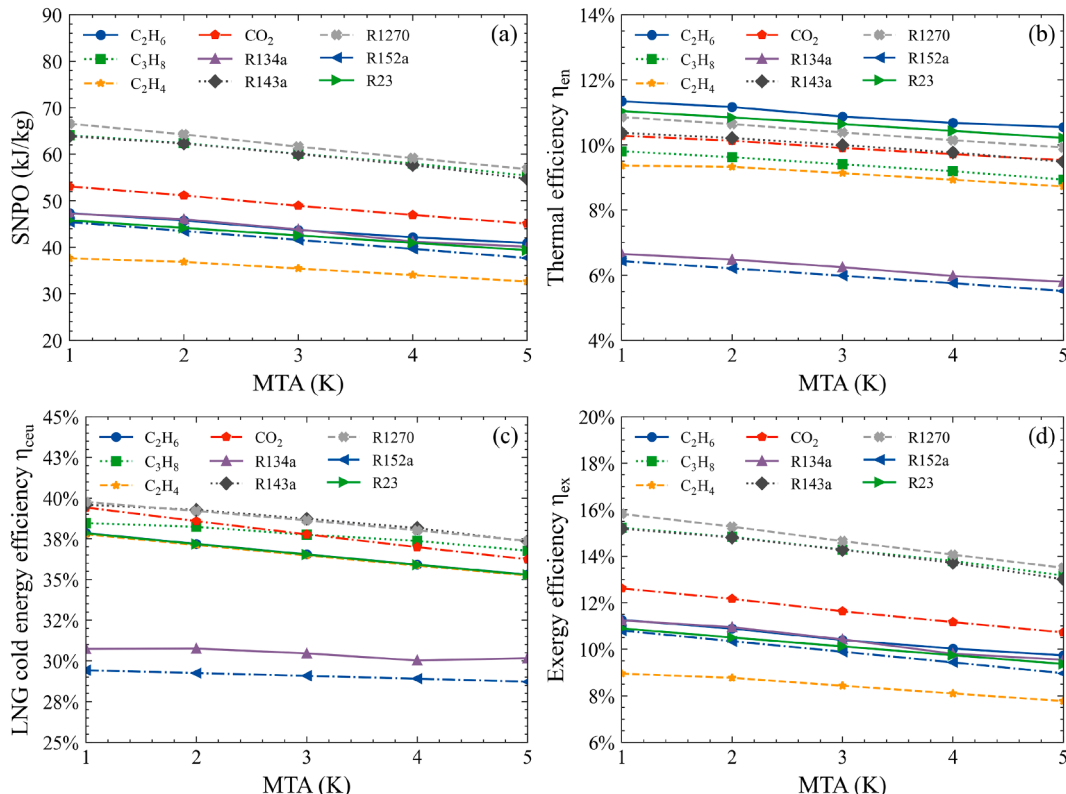


Fig. 6. SNPO (a), thermal efficiency (b), LNG cold exergy utilization efficiency (c) and exergy efficiency (d) for nine potential single-component working fluids and SW T = 25 °C and LNG pressure = 7000 kPa.

4.4. Optimal working fluid selection

According to the above analyses, R1270 has the highest SNPO and exergy efficiency regardless of the variations of the LNG vaporization pressure, seawater temperature and MTA. In other cases, C₂H₆ shows the highest thermal efficiency among nine single working fluids. Since the objective is to maximize the SNPO, R1270 is considered as the optimal single working fluid for the SORC-LNG system. The detailed system performance using R1270 as working fluid is discussed in the following.

Table 5 shows the decision variables and performance indicators of the SORC-LNG using R1270 as working fluid at different LNG vaporization pressures, seawater temperatures and MTAs. Regardless of LNG vaporization pressure variation, the condensation and evaporation pressure of R1270 remain at 110 kPa and 981 kPa. Because the lower bound of condensation pressure is 110 kPa to avoid vacuum condition and the evaporation pressure is determined by the seawater temperature. As the LNG vaporization pressure increases, R1270 M flowrate decreases due to the reduction of the available LNG cold exergy. Furthermore, the exergy destruction decreases from 400.34 kW to 340.27 kW when the LNG vaporization pressure increases from 4000 kPa to 10000 kPa.

By investigating the effect of the seawater temperature on the system performance, it can be seen that the evaporation pressure increases from 743 kPa to 1270 kPa when the seawater temperature increases from 15 °C to 35 °C. However, R1270 molar flowrate remains nearly unchanged. The exergy destruction also increases as the input exergy from seawater rises.

With the increase of the MTA in heat exchangers, the evaporation pressure of R1270 decreases from 1032 kPa to 929 kPa and the molar flowrate decreases from 103.71 kmole/h to 97.42 kmole/h. The reason is that the evaporation temperature reduces with the MTA, leading to a decrease in the evaporation pressure. In addition, with larger MTA, less exergy could be utilized by the SORC-LNG system, which results in a smaller molar flowrate of R1270.

Fig. 7 illustrates the main performance indicators at seawater

temperature of 25 °C. It seems that the optimal design of the SORC-LNG system using R1270 as the working fluid is obtained with the low LNG vaporization pressure and small MTA. To obtain the SNPO larger than 90 kW, the LNG vaporization pressure and MTA should be smaller than 4200 kPa and 2.7 K, respectively, which is represented by the small triangle area with red color as shown in Fig. 7(a). For the other three indicators, the areas to provide the highest efficiency level are significantly larger than the SNPO. It indicates that the synergistic effect of the LNG vaporization pressure and MTA on the SNPO is much weaker than the other indicators.

Fig. 8 shows the four indicators versus LNG vaporization pressure and seawater temperature. The results imply that the SNPO, thermal efficiency, and exergy efficiency increases with a lower LNG vaporization pressure and higher seawater temperature. However, the LNG cold exergy utilization efficiency is only affected by the LNG vaporization pressure regardless of the variation of the seawater temperature. It can be seen that when the LNG vaporization pressure is 4000 kPa, the SNPO can be larger than 90 kW even if the seawater temperature is 25.5 °C. However, when the LNG vaporization pressure raises to 5200 kPa, the seawater temperature has to be higher than 35 °C to ensure the SNPO is larger than 90 kW. In terms of the thermal efficiency and exergy efficiency, the variation ranges of the LNG vaporization pressure and seawater temperature are much broader than that for the SNPO.

The SNPO, thermal efficiency, LNG cold exergy utilization efficiency and exergy efficiency versus the seawater temperature and MTA is shown in Fig. 9. The SNPO, thermal efficiency and exergy efficiency reach the highest level at smaller MTA and higher seawater temperature. However, the range of the seawater temperature and MTA to reach the highest level for the SNPO is broader than those for the thermal efficiency and exergy efficiency, as can be seen in Figs. 7 and 8.

4.5. Performance enhancement by binary mixed working fluids

Having considered using single working fluids to utilize LNG cold energy in the SORC-LNG system, it is fascinating to investigate what opportunity it can provide to enhance system performance by mixing

Table 5

The decision variables and performance indicators of the SORC-LNG system using R1270 as working fluid.

P _{LNG} (kPa)	MTA (K)	T _{SW} (°C)	\dot{n}_{R1270} (kmole/h)	P _{WF-4} (kPa)	P _{WF-2} (kPa)	SNPO (kJ/kg)	η_{en}	η_{ceu}	η_{ex}	$\Delta\dot{E}_d$ (kW)
Effect of the LNG vaporization pressure										
4000	3	25	124.72	110.00	981.00	89.34	12.29%	40.77%	18.96%	400.34
5000	3	25	118.03	110.00	981.00	80.93	11.76%	40.90%	18.25%	380.76
6000	3	25	110.60	110.00	981.00	71.87	11.15%	40.24%	17.05%	367.40
7000	3	25	101.83	110.00	981.00	61.64	10.38%	38.63%	15.27%	359.02
8000	3	25	93.45	110.00	981.00	51.74	9.50%	36.77%	13.33%	353.09
9000	3	25	88.16	110.00	981.00	44.57	8.67%	35.84%	11.89%	346.59
10000	3	25	84.55	110.00	981.00	38.86	7.88%	35.38%	10.70%	340.27
Effect of the seawater temperature										
7000	3	15	100.50	110.00	743.00	50.57	8.68%	38.63%	12.53%	343.36
7000	3	20	101.04	110.00	856.00	56.27	9.57%	38.63%	13.94%	351.16
7000	3	25	101.83	110.00	981.00	61.64	10.38%	38.63%	15.27%	359.02
7000	3	30	100.87	110.00	1118.00	67.05	11.19%	38.63%	16.62%	366.58
7000	3	35	101.24	110.00	1270.00	71.97	11.91%	38.63%	17.83%	374.36
Effect of the MTA										
7000	1	25	103.71	110.00	1032.00	66.57	10.85%	39.76%	16.50%	354.19
7000	2	25	102.28	110.00	1007.00	64.26	10.64%	39.21%	15.92%	356.46
7000	3	25	101.83	110.00	981.00	61.64	10.38%	38.63%	15.27%	359.02
7000	4	25	100.14	110.00	955.00	59.17	10.15%	38.02%	14.66%	361.44
7000	5	25	97.42	110.00	929.00	56.80	9.92%	37.38%	14.07%	363.76

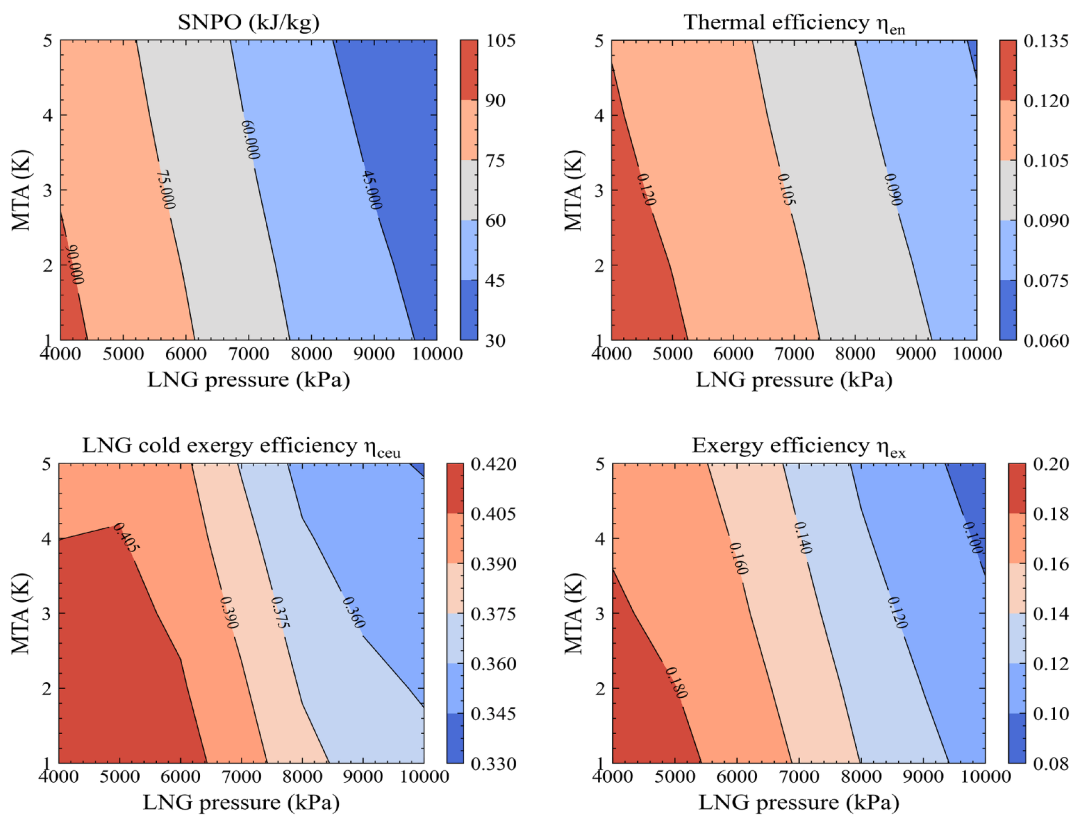


Fig. 7. The contours of SNPO (a), thermal efficiency (b), LNG cold exergy utilization efficiency (c) and exergy efficiency (d) for R1270 versus LNG pressure and MTA.

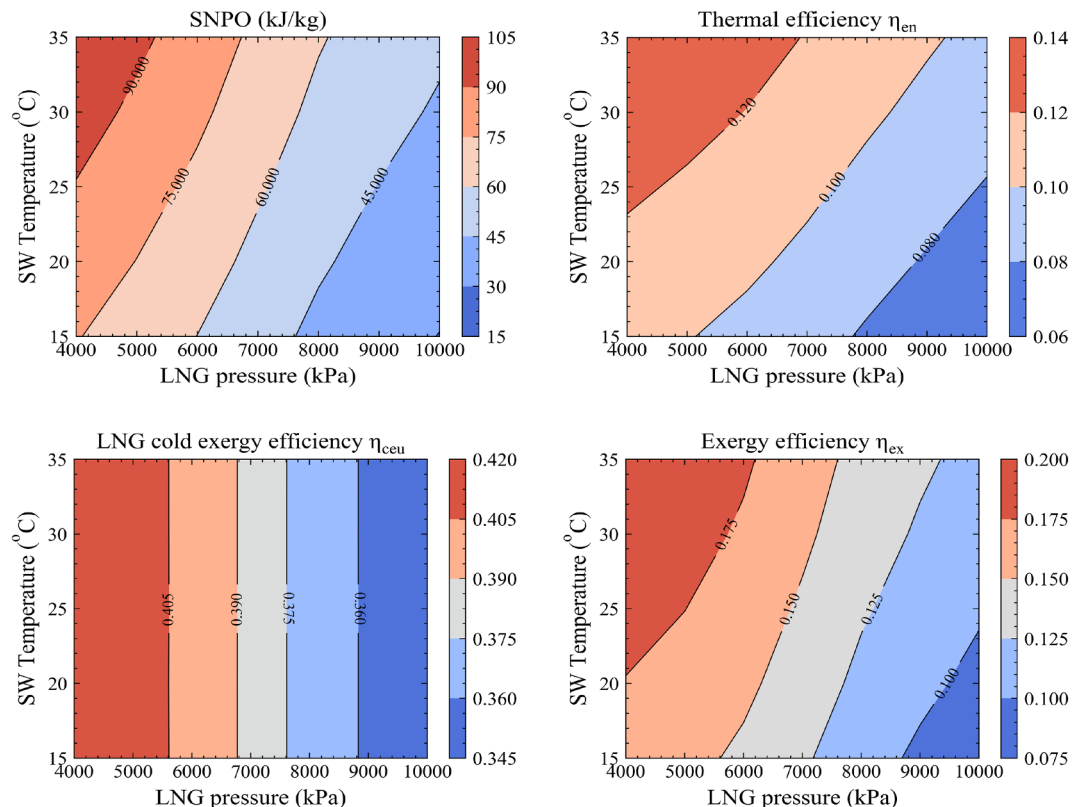


Fig. 8. The contours of SNPO (a), thermal efficiency (b), LNG cold exergy utilization efficiency (c) and exergy efficiency (d) for R1270 versus LNG pressure and SW temperature.

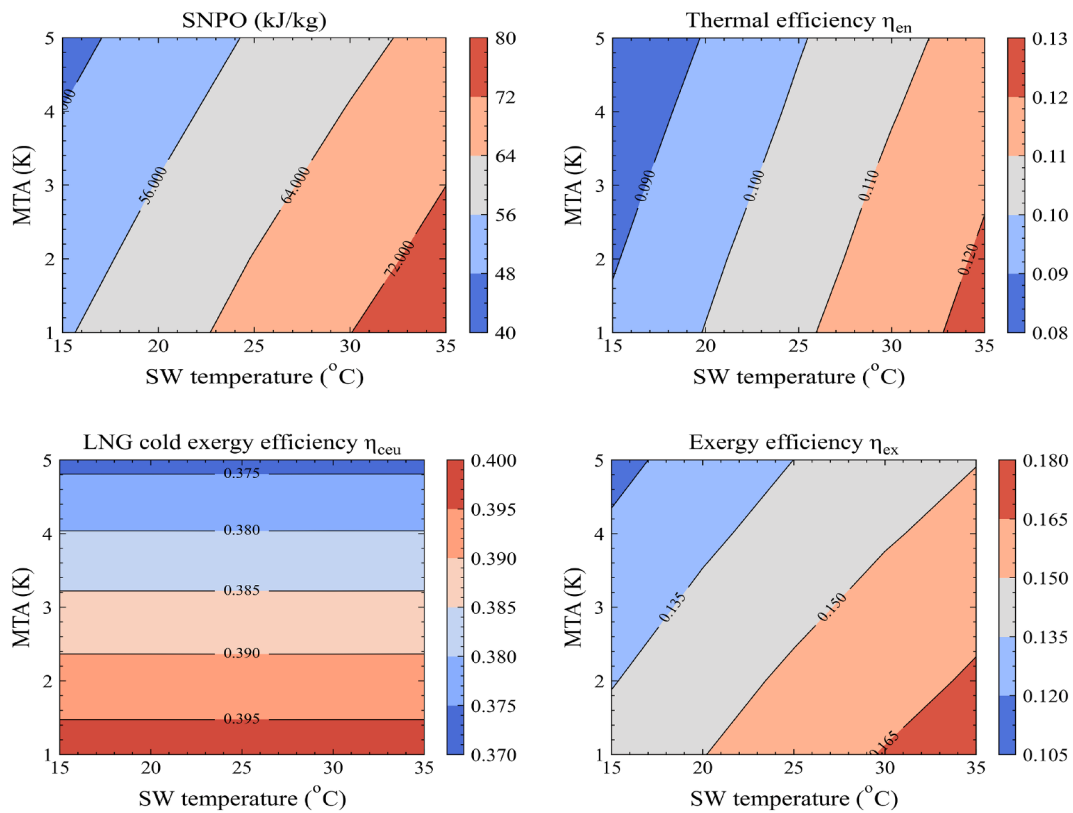


Fig. 9. The contours of SNPO (a), thermal efficiency (b), LNG cold exergy utilization efficiency (c) and exergy efficiency (d) for R1270 versus LNG pressure and SW temperature.

Table 6

The SORC-LNG performance comparison between the single working fluid (R1270) and mixed working fluid (0.4 of R1270 and 0.6 of C₂H₆).

Parameters	$x_{R1270} = 1$	$x_{R1270} : x_{C_2H_6} = 0.4 : 0.6$
\dot{n}_{WF-1} (kmole/h)	101.83	116.55
P_{WF-4} (kPa)	110.00	226.15
P_{WF-2} (kPa)	981.00	2022.07
SNPO (kJ/kg)	61.64	64.85
η_{en}	10.38%	10.94%
η_{ceu}	38.63%	44.80%
η_{ex}	15.27%	16.07%
$\Delta\dot{E}_d$ (kW)	359.02	355.88

these fluids. Mixed working fluids presents a better thermal match with LNG and heat source in the ORC system because of their temperature glide during isobaric condensation and evaporation and thereby results in a smaller exergy destruction and larger net power output.

From the above analysis, R1270 shows the highest SNPO and exergy efficiency and C₂H₆ leads to cycle design with the highest thermal efficiency. Thus, we start the inspection of binary mixed working fluid

(R1270 and C₂H₆) for the SORC-LNG system. The binary mixed working fluid here and hereafter is defined on a molar fraction basis.

The performance comparisons between the single working fluid (R1270) and mixed working fluid at 7000 kPa LNG vaporization pressure, 3 K MTA, and 25 °C seawater temperature, are shown in Table 6. The optimal molar fraction for the mixed working fluid is 0.4 of R1270 and 0.6 of C₂H₆ with the molar flowrate of 116.55 kmole/h, which is 14.45% larger than that of R1270. The condensation pressure and evaporation pressure of the mixed working fluid are higher than the single working fluid. In addition, the LNG cold exergy utilization efficiency by using mixed working fluid is increased by 15.97% indicating that the condensation curve of mixed working fluid could match the LNG evaporation curve better due to the non-isothermal condensation, as shown in Fig. 10(a). The exergy destruction incurred by adopting mixed working fluid is 355.88 kW, which is only 0.87% lower than the single working fluid.

The heat transfer curves in the condenser and evaporator have a significant impact on the SORC-LNG system performance. Fig. 10 illustrates the condensation and evaporation process of the mixed working fluid and R1270 in HEX-1 and HEX-2, respectively. The condensation curve of the R1270/C₂H₆ mixture matches the LNG evaporation curve better than that of R1270. This leads to a reduction of 13.6 kW exergy destruction in HEX-1. This benefit is caused by the non-isothermal condensation of the mixed working fluid. However, the evaporation curve of the mixed working fluid does not match the seawater profile

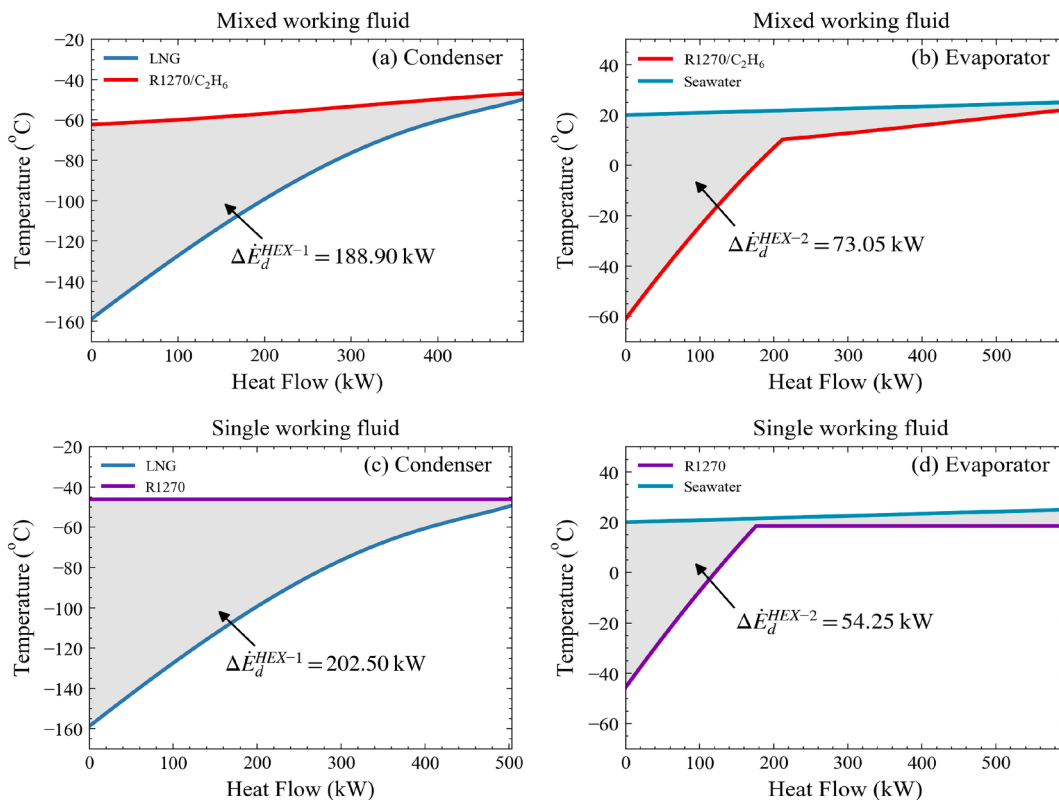


Fig. 10. The heat transfer curves in HEX-1 and HEX-2: (a) LNG and R1270/C₂H₆, (b) R1270/C₂H₆ and seawater, (c) LNG and R1270, (d) R1270 and seawater when the LNG vaporization pressure is 7000 kPa.

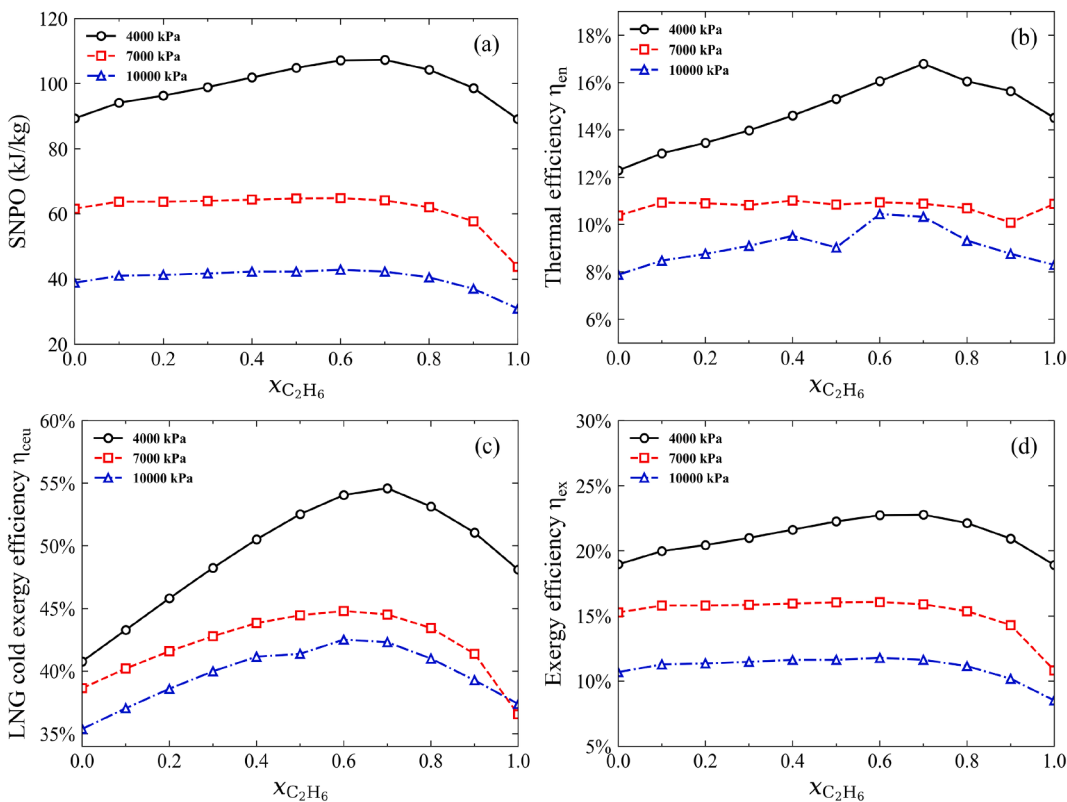


Fig. 11. The performance indicators versus C_2H_6 molar fraction and LNG vaporization pressures when MTA = 3 K and seawater temperature is 25 $^{\circ}\text{C}$.

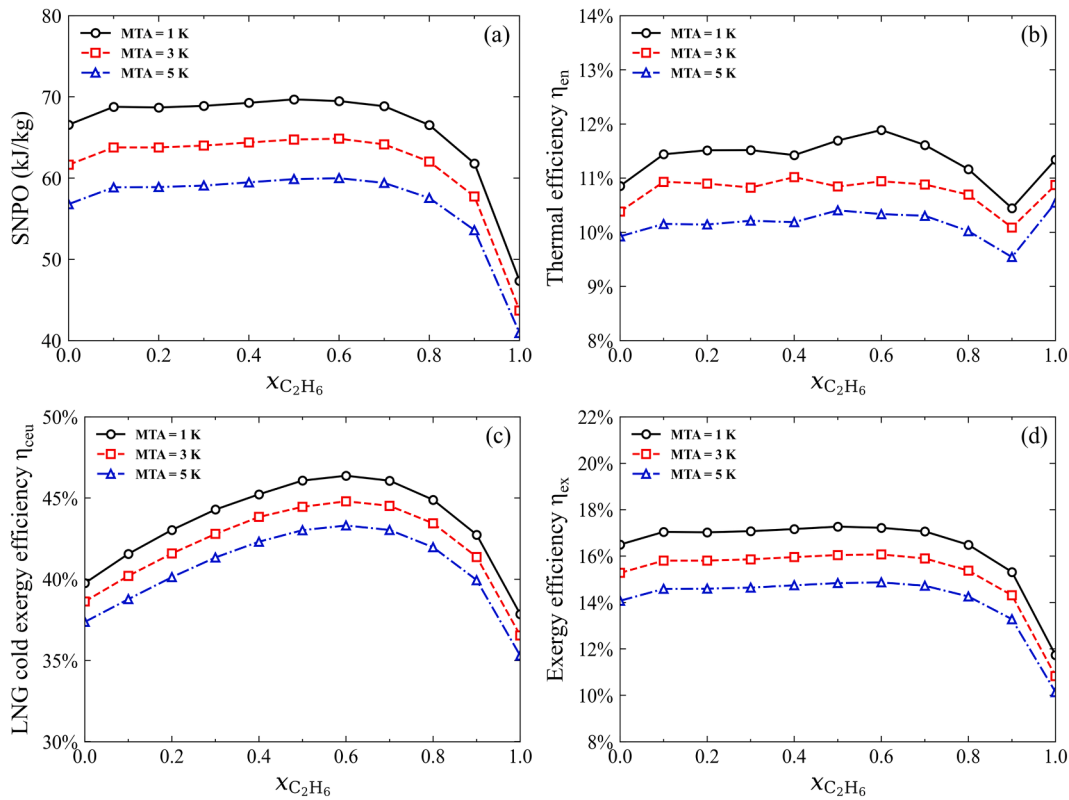


Fig. 12. The performance indicators versus C_2H_6 molar fraction and MTAs.

well due to the non-isothermal evaporation characteristic. The exergy destruction of HEX-2 by using mixed working fluid is 34.67% higher than R1270, as shown in Fig. 10(b) and (d).

The performance indicators versus C_2H_6 molar fraction and LNG vaporization pressure are shown in Fig. 11. It is clear that the SNPO, thermal efficiency, LNG cold exergy utilization efficiency and exergy efficiency first increase and then decrease with the increase of C_2H_6 molar fraction. The optimal system performance is achieved at $x_{C_2H_6} = 0.7$ for 4000 kPa and at $x_{C_2H_6} = 0.6$ for 7000 kPa and 10000 kPa. Moreover, the performance enhancement by R1270/ C_2H_6 is distinctive with different LNG vaporization pressures. Compared to R1270, the increment of the SNPO by adopting R1270/ C_2H_6 as working fluid is 20.11%, 5.21%, and 10.19% for 4000 kPa, 7000 kPa, and 10000 kPa, respectively.

Fig. 12 shows the variations of performance indicators versus C_2H_6 molar fraction and MTAs. The SNPO and exergy efficiency of the SORC-LNG system increase slightly first and then decrease dramatically with the increase of the C_2H_6 molar fraction. The highest SNPO and exergy efficiency at MTA = 1 K is 69.69 kW and 16.56%, respectively. This is 4.68% higher than those of R1270. However, the highest SNPO and exergy efficiency at MTA = 3 K and 5 K are achieved at a C_2H_6 molar fraction of 0.6. It indicates that the optimal molar fraction of the mixed working fluid varies with different MTAs. In terms of the thermal efficiency, it first hits the peak value, then decreases and finally increases as

C_2H_6 molar fraction rises. It means that adopting mixed working fluid in the SORC-LNG system does not always benefit the thermal efficiency. Furthermore, the highest LNG cold exergy utilization efficiency at MTA = 1 K, 3 K and 5 K is 46.37%, 44.80%, and 43.31% at a C_2H_6 molar fraction of 0.6, respectively, which is 16.62%, 15.97%, and 15.89% higher than that adopting pure R1270 as working fluid. The result implies that mixed working fluid could match the LNG evaporation curve better and therefore increase the LNG cold exergy utilization efficiency. Moreover, the smaller MTA, the larger benefit for the LNG cold exergy utilization efficiency.

Fig. 13 demonstrates the variation of the SNPO, thermal efficiency, LNG cold exergy utilization efficiency, and exergy efficiency versus C_2H_6 molar fraction and seawater temperature. Their variation trends are similar with Fig. 12. The only difference is that the LNG cold exergy utilization efficiency is almost the same for the seawater temperature at 15 °C, 25 °C, and 35 °C, as shown in Fig. 11(c).

From Figs. 10–13, we can draw some conclusions concerning the performance enhancement by adopting mixed working fluid. For the case of lower LNG vaporization pressure (4000 kPa), the SNPO, thermal efficiency, LNG cold exergy utilization efficiency, and exergy efficiency are improved significantly by using binary mixed working fluid. However, with a higher LNG vaporization pressure (7000 kPa and 10000 kPa), the performance enhancement is marginal by mixing the working fluids with the highest SNPO (R1270) and thermal efficiency (C_2H_6).

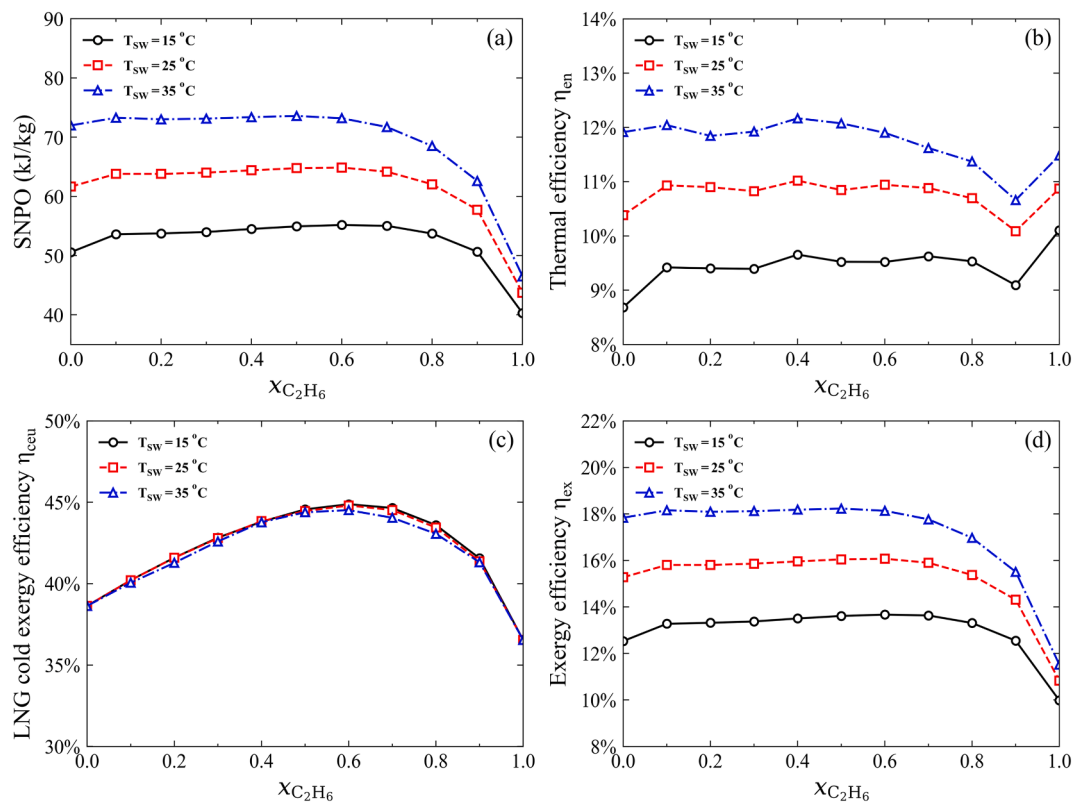


Fig. 13. The performance indicators versus C_2H_6 molar fraction and seawater temperatures.

5. Conclusions

This paper conducted a comprehensive study to investigate the effects of LNG vaporization pressure, seawater temperature, MTA, and working fluid selection on SORC-LNG performance by global optimization using PSO. The energetic and exergetic analyses of nine single working fluids were carried out for different LNG vaporization pressures, seawater temperatures, and MTAs. Moreover, the performance intensification by adopting binary working fluids were studied. The main conclusions and key findings were gained as follows:

1. The LNG vaporization pressure had the most significant influence on the SORC-LNG performance since it determined the evaporation curve and available cold exergy and thereby affected the optimal working fluid.
2. R1270 exhibited the highest SNPO (89.34 kJ/kg) and exergy efficiency (18.96%) among single working fluids while C_2H_6 had the highest thermal efficiency.
3. SNPO, thermal efficiency, LNG cold exergy utilization efficiency, and exergy efficiency were improved by 20.11%, 36.66%, 33.92%, and 20.01%, respectively, by using binary mixture of R1270/ C_2H_6 =0.3/0.7 as working fluid when LNG vaporization pressure was 4000 kPa. However, the performance intensification was marginal for a high LNG vaporization pressure (7000 kPa and 10000 kPa).
4. The non-isothermal condensation of the mixed working fluid could match the LNG evaporation curve appropriately and thereby reduce the exergy destruction in the condensation. However, the non-isothermal evaporation of the mixed working fluid did not always show a better match with the seawater cooling curve and thus resulted in a larger exergy destruction in the evaporator.

This work could provide a theoretical guide to choose appropriate ORC working fluid in future practical applications for LNG terminals with different downstream purposes at different locations. However, several

challenges are still needed to be addressed: (1) dynamic behaviors and part-load performance of the SORC-LNG system should be investigated; (2) economic analysis and life-cycle assessment are also required to illustrate its economical and environmental performance; (3) efficient condenser and evaporator should be designed to reduce the exergy destruction.

CRediT authorship contribution statement

Tianbiao He: Conceptualization, Methodology, Writing - original draft, Funding acquisition. **Huigang Ma:** Visualization, Data curation. **Jie Ma:** Software, Validation. **Ning Mao:** Validation, Investigation. **Zuming Liu:** Supervision.

Declaration of Competing Interest

The authors declare that they have no known competing financial interests or personal relationships that could have appeared to influence the work reported in this paper.

Acknowledgement

The authors would like to appreciate the funding support of the National Natural Science Foundation of China (No. 51906225), the Shandong Provincial Natural Science Foundation (No. ZR2019QEE020), and the Fundamental Research Funds for the Central Universities (No. 19CX02011A).

References

- [1] Ahmadi Mohammad H, Ahmadi Mohammad-Ali, Aboukazempour Esmail, Grosu Lavinia, Pourfayaz Fathollah, Bidi Mokhtar. Exergetic sustainability evaluation and optimization of an irreversible brayton cycle performance. *Front Energy* 2019;13(2):399–410.
- [2] Lin Wensheng, Zhang Na, Gu Anzhong. LNG (liquefied natural gas): A necessary part in china's future energy infrastructure. *Energy* 2010;35(11):4383–91.

- [3] He Tianbiao, Chong Zheng Rong, Babu Ponnivalavan, Linga Praveen. Techno-Economic Evaluation of Cyclopentane Hydrate-Based Desalination with Liquefied Natural Gas Cold Energy Utilization. *Energy Technol* 2020;8(8):1900212.
- [4] He Tianbiao, Liu Zuming, Yonglin Ju, Parvez Ashak Mahmud. A comprehensive optimization and comparison of modified single mixed refrigerant and parallel nitrogen expansion liquefaction process for small-scale mobile LNG plant. *Energy* 2019;167:1–12.
- [5] Zhang Na, Lior Noam, Liu Meng, Han Wei. Coolcep (cool clean efficient power): A novel co2-capturing oxy-fuel power system with lng (liquefied natural gas) coldness energy utilization. *Energy* 2010;35(2):1200–10.
- [6] IGU World LNG Report 2020. Technical report, International Gas Union, 2020.
- [7] Kim Juwon, Noh Yeelyong, Chang Daejun. Storage system for distributed-energy generation using liquid air combined with liquefied natural gas. *Appl Energy* 2018; 212:1417–32.
- [8] Kanbur Baris Burak, Xiang Liming, Dubey Swapnil, Choo Fook Hoong, Duan Fei. Cold utilization systems of lng: A review. *Renew Sust Energ Rev* 2017;79:1171–88.
- [9] Wang Bojie, Wang Wen, Qi Chao, Kuang Yiwu, Jiawei Xu. Simulation of performance of intermediate fluid vaporizer under wide operation conditions. *Front Energy* 2020;14(3):452–62.
- [10] Xue Feier, Chen Yu, Ju Yonglin. A review of cryogenic power generation cycles with liquefied natural gas cold energy utilization. *Front Energy* 2016;10(3): 363–74.
- [11] Zhao Liang, Dong Hui, Tang Jiajun, Cai Jiujun. Cold energy utilization of liquefied natural gas for capturing carbon dioxide in the flue gas from the magnesite processing industry. *Energy* 2016;105:45–56.
- [12] Tsatsaronis G, Morosuk T. Advanced exergetic analysis of a novel system for generating electricity and vaporizing liquefied natural gas. *Energy* 2010;35(2): 820–9.
- [13] Cao Wensheng, Beggs Clive, Mujtaba Iqbal M. Theoretical approach of freeze seawater desalination on flake ice maker utilizing lng cold energy. *Desalination* 2015;355:22–32.
- [14] Lin Wensheng, Huang Meibin, Gu Anzhong. A seawater freeze desalination prototype system utilizing LNG cold energy. *Int J Hydrogen Energ* 2017;42(29): 18691–8.
- [15] Mehrpooya Mehdi, Kalhorzadeh Masoud, Chahartaghi Mahmood. Investigation of novel integrated air separation processes, cold energy recovery of liquefied natural gas and carbon dioxide power cycle. *J Cleaner Production* 2016;113:411–25.
- [16] Lee Inkyu, You Fengji. Systems design and analysis of liquid air energy storage from liquefied natural gas cold energy. *Appl Energy* 2019;242:168–80.
- [17] He Tianbiao, Lv Hongyu, Shao Zixian, Zhang Jibao, Xing Xialian, Ma Huigang. Cascade utilization of LNG cold energy by integrating cryogenic energy storage, organic Rankine cycle and direct cooling. *Appl Energy* 2020;277:115570.
- [18] Mehrpooya Mehdi, Sharifzadeh Mohammad Mehdi Moftakhar, Katooli Mohammad H. Thermodynamic analysis of integrated LNG regasification process configurations. *Progress Energy Combustion Sci* 2018;69:1–27.
- [19] Angelino Gianfranco, Invernizzi Costante M. The role of real gas brayton cycles for the use of liquid natural gas physical exergy. *Appl Thermal Eng* 2011;31(5): 827–33.
- [20] Gómez Manuel Romero, García Ramón Ferreiro, Gómez Javier Romero, Carril José Carbia. Thermodynamic analysis of a brayton cycle and rankine cycle arranged in series exploiting the cold exergy of LNG (liquefied natural gas). *Energy* 2014;66: 927–37.
- [21] Ghaebi Hadi, Parikhani Towhid, Rostamzadeh Hadi. Energy, exergy and thermoeconomic analysis of a novel combined cooling and power system using low-temperature heat source and lng cold energy recovery. *Energy Conversion Management* 2017;150:678–92.
- [22] Parikhani Towhid, Gholizadeh Towhid, Ghaebi Hadi, Sadat Seyed Mohammad Sattari, Sarabi Mehrdad. Exergoeconomic optimization of a novel multigeneration system driven by geothermal heat source and liquefied natural gas cold energy recovery. *J Cleaner Production* 2019;209:550–71.
- [23] Lee Ung, Park Keonhee, Jeong Yeong Su, Lee Sangho, Han Chonghun. Design and analysis of a combined rankine cycle for waste heat recovery of a coal power plant using lng cryogenic exergy. *Ind Eng Chem Res* 2014;53(23):9812–24.
- [24] Li Xiaoya, Song Jian, Yu Guopeng, Liang Youcui, Hua Tian, Shu Gequn, et al. Organic Rankine cycle systems for engine waste-heat recovery: Heat exchanger design in space-constrained applications. *Energ Convers Manage* 2019;199: 111968.
- [25] Zhang Xuelin, Zhang Tong, Xue Xiaodai, Si Yang, Zhang Xuemin, Mei Shengwei. A comparative thermodynamic analysis of kalina and organic rankine cycles for hot dry rock: a prospect study in the gonghe basin. *Front. Energy* 2020;14(4): 889–900.
- [26] Song Jian, Li Xiaoya, Wang Kai, Markides Christos N. Parametric optimisation of a combined supercritical co2 (s-co2) cycle and organic rankine cycle (orc) system for internal combustion engine (ice) waste-heat recovery. *Energy Conversion Management* 2020;218:112999.
- [27] Liu Zuming, He Tianbiao. Exergoeconomic analysis and optimization of a Gas Turbine-Modular Helium Reactor with new organic Rankine cycle for efficient design and operation. *Energy Conversion Management* 2020;204:112311.
- [28] Tsougrakis Emmanouil-Loizos, Dawei Wu. Dual Reutilization of LNG Cryogenic Energy and Thermal Waste Energy with Organic Rankine Cycle in Marine Applications. *Energy Procedia* 2017;142:1401–6.
- [29] He Tianbiao, Chong Zheng Rong, Zheng Junjie, Ju Yonglin, Linga Praveen. LNG cold energy utilization: Prospects and challenges. *Energy* 2019;170:557–68.
- [30] García Ramón Ferreiro, Carril José Carbia, Gomez Javier Romero, Gomez Manuel Romero. Combined cascaded rankine and direct expander based power units using lng (liquefied natural gas) cold as heat sink in LNG regasification. *Energy* 2016; 105:16–24.
- [31] Bao Junjiang, Lin Yan, Zhang Ruixiang, Zhang Ning, He GaoHong. Strengthening power generation efficiency utilizing liquefied natural gas cold energy by a novel two-stage condensation Rankine cycle (TCRC) system. *Energy Conversion Management* 2017;143:312–25.
- [32] Sun Zhixin, Zhang Han, Zhang Tianfeng, Lin Li, Lin Kui. Optimizations and comparison of three two-stage Rankine cycles under different heat source temperatures and NG distribution pressures. *Energ Convers Manage* 2020;209: 112655.
- [33] Tomkow Łukasz, Cholewiński Maciej. Modelling of a novel power-generating cycle for the utilization of the cold exergy of liquid natural gas with the adjustable parameters of working fluid. *Energy Conversion Management* 2019;201:112178.
- [34] Sun Qingxuan, Wang Yaxiong, Cheng Ziyang, Wang Jiangfeng, Zhao Pan. Thermodynamic and economic optimization of a double-pressure organic Rankine cycle driven by low-temperature heat source. *Renew Energ* 2020;147:2822–32.
- [35] Bao Junjiang, Zhang Ruixiang, Yuan Tong, Zhang Xiaopeng, Zhang Ning, He GaoHong. A simultaneous approach to optimize the component and composition of zeotropic mixture for power generation systems. *Energy Conversion Management* 2018;165:354–62.
- [36] Sung Taehong, Kim Kyung Chun. Thermodynamic analysis of a novel dual-loop organic Rankine cycle for engine waste heat and LNG cold. *Appl Thermal Eng* 2016;100:1031–41.
- [37] He Tianbiao, Zhang Jibao, Mao Ning, Linga Praveen. Organic rankine cycle integrated with hydrate-based desalination for a sustainable energy–water nexus system. *Appl Energy* 2021;291:116839.
- [38] Xue Feier, Chen Yu, Ju Yonglin. Design and optimization of a novel cryogenic Rankine power generation system employing binary and ternary mixtures as working fluids based on the cold exergy utilization of liquefied natural gas (LNG). *Energy* 2017;138:706–20.
- [39] He Tianbiao, Nair Sajitha K, Babu Ponnivalavan, Linga Praveen, Karimi Iftekhar A. A novel conceptual design of hydrate based desalination (HyDesal) process by utilizing LNG cold energy. *Appl Energy* 2018;222:13–24.
- [40] He Tianbiao, Mao Ning, Liu Zuming, Qyyum Muhammad Abdul, Lee Moonyong, Pravez Ashak Mahmud. Impact of mixed refrigerant selection on energy and exergy performance of natural gas liquefaction processes. *Energy* 2020;199:117378.
- [41] Aspen HYSYS V10.0. <https://www.aspentechn.com/>. 2017.
- [42] Peng Ding-Yu, Robinson Donald B. A new two-constant equation of state. *Ind Eng Chem Fundamentals* 1976;15(1):59–64.
- [43] Chen Chau-Chyun, Song Yuhua. Generalized electrolyte-NRTL model for mixed-solvent electrolyte systems. *AIChE J* 2004;50(8):1928–41.
- [44] MathWorks. <https://www.mathworks.com/>. 2018.